DC Shipboard Microgrid Modeling for Fuel Cell Integration Study

F. D'Agostino, G. P. Schiapparelli, F. Silvestro
University of Genoa
Department of Electrical, Electronic, Telecommunication Engineering and Naval Architecture
Via all'Opera Pia 11 A
I-16145, Genova, Italy
{fabio.dagostino,giacomo-piero.schiapparelli}@edu.unige.it,
federico.silvestro@unige.it

S. Grillo
Politecnico di Milano
p.za Leonardo da Vinci, 32
Dipartimento di Elettronica, Informazione e Bioingegneria
I-20133, Milano, Italy
samuele.grillo@polimi.it

***Abstract*—The integration of fuel cell technology in shipboard is essential for real fuel and pollution reduction in the marine sector. This integration can be pushed in the adoption of a dc shipboard power system (SPS). One of the impediments to this integration is the necessity to couple fuel cells (FCs) and battery energy storage systems (BESSs) and control them with a proper power management system (PMS), in order to sustain high load variations due to electric propulsion. In the literature, all these aspects are dealt independently and mostly assuming ideal conditions. The proposed control strategies are derived from the droop and secondary frequency regulation of the ac power system. This paper starts with a brief description on the characteristics of dc SPS along with fuel cell and battery modeling. Subsequently, this paper describes the proposed control strategy. Finally, this paper shows the behavior and principle of the proposed integration and analyzes the performance on a real measurement test case of a ferry. This paper is concluded by identifying the future research for the development of a PMS control strategy for critical marine missions.**

***Index Terms*—dc microgrids, shipboard power system, power management system, voltage deviations, droop control.**

I. Introduction

Recently, shipboard electric power systems have been studied with growing attention. In fact, there have been a continuous trend in ship electrification, going towards the "all electric ship" [1], and following this paradigm, ships become one the most demanding instance of microgrids [2].

Along with this shift in electrification, shipboard microgrids are also moving from traditional ac distribution systems to dc distribution systems [3]. In fact, while the former are broadly deployed, the latter have many advantages as they seamlessly integrate dc-native loads and generation (e.g., photovoltaic generation, and energy storages), improve efficiency in case of variable speed drives, and need simpler management strategies (i.e., they do not need either reactive power or frequency control and are less prone to harmonic disturbances) [4], [5]. On the other hand, it must be noted that protection of dc systems must be thoroughly studied in order to attain the security and selectivity performances of ac systems [6], [7].

While designing and implementing dc microgrids, one of the main issues is the coordination of the various power converters connected to the common dc-bus. This coordination is directly connected to the energy management of the whole microgrid. The most common way to achieve this result is to exploit the droop controllers [8]–[10]. The observed variable is the dc-bus voltage and the deviations from the rated, desired, value are used to activate the intervention of the different devices connected to the dc-bus in order to keep its voltage as constant and smooth as possible.

In particular, shipboard microgrids—isolated by nature—are characterized by the simultaneous presence of "slow-reacting" generators (e.g., diesel units, fuel cells) and loads with high dynamics (e.g., the propulsion system, especially when maneuvering). In this cases, devices (e.g., battery energy storage systems, BESSs) able to rapidly supply loads are needed along with a suitable control strategy for effectively decoupling the contributions.

In [11] a strategy for controlling diesel generators, BESSs, loads, and the shore connection is described. BESSs are used to limit large voltage deviations on the dc-bus by taking charge of fast load ramp rates. However, even if the amount of information to be exchanged between power converters is reduced, there is still need for a direct communication among converters. This may cause delays and problems, possibly jeopardizing stability and power supply security in real operation.

This work investigates the effectiveness of a control strategy for the combined operation of fuel cells and BESSs in a dc shipboard system using the voltage of the dc-bus (i.e., the error with respect to the reference value) as the control signal. In this way, there is no need to send additional signals among converters, thus increasing robustness. Therefore, dc-bus voltage takes the role of the frequency in ac distribution systems.

The paper is structured as follows. In Section II the components of the shipboard power system model are described. Section III details the control system architecture, whose

IEEE Power and Energy Society General Meeting, Article number 8973461 DOI: https://doi.org/10.1109/PESGM40551.2019.8973461

effectiveness is validated in Section IV, considering the previously described classical shipboard microgrid using both an "synthetic" load profile—specifically designed to show the behavior of the control strategy—and a real load profile as registered during a 33-minute operation of a ferry vessel [12]. Finally, some conclusions and future developments are drawn in Section V.

II. System model

The shipboard power plant is made up of three dc-busbars (port, PS, center CS, and starboard, STB). The two propulsion motors, as well as the two BESSs and two of the three proton exchange membrane fuel cells (PEMFCs) are connected to the port and to the starboard bus, respectively. The ac hotel load, and the third PEMFC are connected with the center bus, (see Fig. 1).

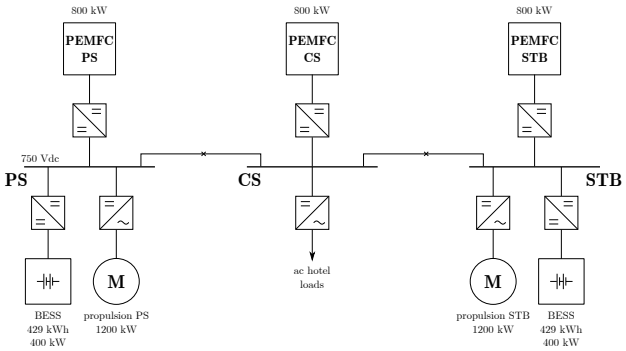

Figure 1. One line diagram of the case study grid.

A. Fuel Cell Dynamic Model

The PEMFC dynamic model is designed as in [13]. PEMFCs have a high power density and offer the advantage of reduced weight and volume compared to other types of cells. They operate at relatively low temperatures, allowing them to be started quickly and to be used for longer duration. The dynamic behavior of a PEMFC generating system can be separated in three different sections: i) fuel compressor, ii) power section, and iii) power conditioning system.

A notable impediment to use them on ships is hydrogen storage. In fact, it must be provided on board as compressed gas in pressurized tanks. The fuel compressor is necessary to extract and preheat the hydrogen and oxygen that is required to the PEMFCs. This process is particularly delicate as the cells are sensitive to impurities [14]. The modelling of the fuel processor is assumed as a delay, T_{D}. The power section (as depicted in Fig. 2) models the PEMFC cell reactions. The modelling is based on some assumptions: 1) Nernst's equation holds true, 2) the gas can be considered as ideal, 3) the cell temperature can be considered stable during all the time, 4) the pressure drop across the electrode channels is negligible, 5) the pressure ratio between inside and outside of the electrode channel is assumed to be large enough to consider a chocked flow, and 6) the activation and ohmic losses are taken into account [13]. Figure 2 shows the block diagram of the dynamic model of the power section of the PEMFC as described in [13]. The potential difference between the anode and the cathode is calculated using Nernst's equation and Ohm's law to take into account activation and ohmic losses:

$$V_{\mathrm{module}} = N_{\mathrm{s}} \left[E_0^{\mathrm{FC}} + \frac{RT}{2F} \ln \left(\frac{\rho_{\mathrm{H_2}} \rho_{\mathrm{O_2}}^{0.5}}{\rho_{\mathrm{H_2O}}} \right) \right] + -R_{\mathrm{int}}^{\mathrm{FC}} I - B^{\mathrm{FC}} \ln (CI), \quad (1)$$

where N_{s} is the no. of cells in series, E_0^{FC} is the no-load voltage, R is the universal gas constant, F is the Faraday constant, T is the stack temperature, $\rho_{(\cdot)}$'s are the derivatives of the partial pressures of the fluids, $R_{\mathrm{int}}^{\mathrm{FC}}$ is the internal resistance, I is the cell current, and B^{FC} and C are the voltage activation constants.

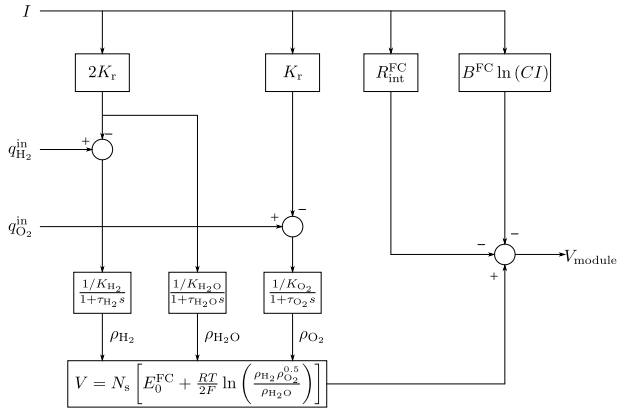

Figure 2. Dynamic model of the power section of a single PEMFC module.

The ideal gas law allows to find out the partial pressures of the gases flowing through the electrodes. In following equations, tables, and figures $q_{(\cdot)}^{\mathrm{in}}$'s are gases inflows, $K_{(\cdot)}$'s and $\tau_{(\cdot)}$'s are the valve and time delays of each circuit. The equation of hydrogen flow can be used to calculate the derivative of the partial pressure of the hydrogen taking into account the relation between hydrogen inflow and I:

$$\rho_{\mathrm{H_2}} = \frac{1/K_{\mathrm{H_2}}}{1 + \tau_{\mathrm{H_2}} s} \left(q_{\mathrm{H_2}}^{\mathrm{in}} - 2K_{\mathrm{r}} I \right) \quad (2)$$

where $K_{\mathrm{r}} = N_{\mathrm{s}}/(4F)$.

The power conditioning system consists in a dc-dc buck converter that is regulated by the control signal, α, which is defined as the ratio of the voltages on the dc-bus side and on the fuel cell side. The circuit has been implemented in DIgSILENT PowerFactory simulation environment. The main parameters of the 100 kW PEMFC module as in [13] are reported in Table I. Therefore, each 800 kW-700 V PEMFC generator, is obtained with 4 parallel stacks composed by a series of 2 modules each.

B. Battery model

According to [15], [16] a battery can be modeled as a voltage source in series with a resistance (see Fig. 3). Thus,

Table I
PARAMETERS OF THE 100 kW PEMFC MODULE [13].

Parameter	Value
T	343 K
E_0^{FC}	0.8 V
no. of cells in series N_s	550
no. of parallel cells N_p	6
$K_r = N_0/(4F)$	1.4251×10^{-6} kmol s^{-1}
$K_{\mathrm{H_2}}$	4.22×10^{-5} kmol s^{-1} atm^{-1}
$K_{\mathrm{H_2O}}$	7.716×10^{-6} kmol s^{-1} atm^{-1}
$K_{\mathrm{O_2}}$	2.11×10^{-5} kmol s^{-1} atm^{-1}
$\tau_{\mathrm{H_2}}$	3.37 s
$\tau_{\mathrm{H_2O}}$	18.418 s
$\tau_{\mathrm{O_2}}$	6.74 s
B^{FC}	0.047 77 A^{-1}
C	0.0136 V
$R_{\mathrm{int}}^{\mathrm{FC}}$	0.2778 Ω
T_d	2 s

Table II
PARAMETERS OF THE BESS USED IN THE CASE STUDY.

Parameter		Value
tray	nominal voltage	58.4 V
	capacity	68 A h
BESS	no. series trays (=1 rack)	12
	no. parallel racks	9
	nominal energy	429 kWh
	nominal power	400 kW
	max. power @4C	1.71 MW
model	E_0^{B}	700.8 V
	Q	612 Ah
	$R_{\mathrm{int}}^{\mathrm{B}}$ (supposed)	10 mΩ
	K^{B}	8.76 mV
	A	0.468 V
	B	3.5294 Ah^{-1}

applying the Kirchhoff's voltage law, the battery voltage V_{bat} is given by:

$$V_{\mathrm{bat}} = E_{\mathrm{bat}} - R_{\mathrm{int}}^{\mathrm{B}} I_{\mathrm{bat}} \tag{3}$$

$$E_{\mathrm{bat}} = E_0^{\mathrm{B}} - K\frac{1-\mathrm{SOC}}{\mathrm{SOC}}Q + A\exp\left(-B^{\mathrm{B}}\left(1-\mathrm{SOC}\right)Q\right), \tag{4}$$

where E_0^{B} is the battery open-circuit nominal voltage [V], K^{B} is the polarization voltage [V], Q is the battery capacity [Ah], SOC is the state of charge (in p.u.) calculated starting from an initial (known) value (SOC_0 by using any SOC estimation technique (for instance the Coulomb-counting method, $\mathrm{SOC}\left(t\right) = \mathrm{SOC}_0 - \frac{\int_0^t I_{\mathrm{bat}}(\tau)d\tau}{Q}$), A is the exponential zone amplitude [V], and B^{B} is the exponential zone time constant inverse [Ah^{-1}].

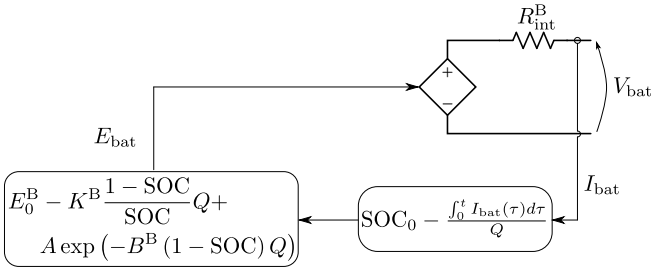

Figure 3. Model of the battery [11].

The BESS used for the study case is a 429 kW h Lithium Nickel Manganese Cobalt Oxide (NCM) battery, made up of 9 parallel racks each of which containing 12 series trays. The key parameters of each BESS are reported in Table II.

III. POWER CONTROL STRATEGY

The proposed power control strategy is based on primary and secondary frequency regulation concepts, applied to a single dc-busbar power system. The basic idea is to use the dc-busbar voltage deviation as the power unbalance signal, similarly to the primary frequency-power regulation basics for classical ac power systems. The major hypothesis for the applicability of the proposed power control strategy is to consider that each power generating unit is connected to the same electrical node, in order to allow the adoption of the node voltage as the common signal for all the installed devices. This hypothesis is verified by the single-busbar architecture, which is extremely common in shipboard applications.

The control system architecture is composed by three controllers that implement the system voltage and power regulation: i) dc-bus voltage controller, ii) fuel cell power controller, and iii) secondary voltage controller.

The primary dc-bus voltage regulation is provided by the BESSs, through the dc-bus droop voltage controller, while the secondary control is assigned to the PEMFCs and it is based on an integral controller. The numerical values of the control parameters described in the following subsections are reported in Table III.

A. DC-bus Voltage Controller

A proportional-integral regulator implements the primary dc-bus voltage control provided by the BESS. Each BESS is interfaced by a bi-directional dc-dc boost-buck converter, driven by the control signal α_{B}, which is defined as the ratio of the voltages on the dc-bus side and on the battery side.

The regulation action provided by the dc-bus voltage controller, i.e., the control signal alpha variation for each BESS is given by:

$$\Delta\alpha_{\mathrm{B}} = \left(K_{\mathrm{p}}^{\mathrm{B}} + \frac{K_{\mathrm{i}}^{\mathrm{B}}}{s}\right)\left(v_{\mathrm{ref}} - v\right), \tag{5}$$

where $K_{\mathrm{p}}^{\mathrm{B}}$ and $K_{\mathrm{i}}^{\mathrm{B}}$, are regulator proportional and integral gains respectively, v_{ref} is the reference voltage, and v is the actual dc-bus voltage.

When the load increases, the dc-bus voltage drops as a consequence of the current increasing. The dc-bus voltage

controller provides the α_{B} signal adjustment, and the power produced by the battery increases.

In order to use the voltage deviation as the load-change signal, the reference voltage v_{ref} is provided by a droop controller:

$$v_{\mathrm{ref}} = v_{\mathrm{n}} + D_{\mathrm{v}} \left(p^{\mathrm{B}}_{\mathrm{ref}} - p^{\mathrm{B}}_{\mathrm{act}} \right), \tag{6}$$

where v_{n} is the nominal dc-bus voltage, $p^{\mathrm{B}}_{\mathrm{ref}}$ and $p^{\mathrm{B}}_{\mathrm{act}}$ are the BESS power reference and actual power respectively, and D_{v} is the voltage droop coefficient.

B. Fuel Cell Power Controller

Each PEMFC is connected to the dc bus by means of a dc-dc boost converter, driven by the control signal alpha (α_{FC}), which is defined as the ratio of the voltages on the dc-bus side and on the generator side. The generator power control is implemented by a proportional-integral regulator fed by the power deviation from a defined reference value:

$$\Delta\alpha_{\mathrm{FC}} = \left(K^{\mathrm{FC}}_{\mathrm{p}} + \frac{K^{\mathrm{FC}}_{\mathrm{i}}}{s} \right) \left(p^{\mathrm{FC}}_{\mathrm{ref}} - p^{\mathrm{FC}}_{\mathrm{act}} \right) \tag{7}$$

where $K^{\mathrm{FC}}_{\mathrm{p}}$ and $K^{\mathrm{FC}}_{\mathrm{i}}$, are the regulator proportional and integral gains respectively, $p^{\mathrm{FC}}_{\mathrm{ref}}$ is the power reference and $p^{\mathrm{FC}}_{\mathrm{act}}$ is the actual power production of the generator.

This local control strategy allows the PEMFC generator to provide constant power, avoiding power flow variations as a consequence of dc-bus voltage fluctuations. The participation into the primary voltage regulation is not compatible with the poor dynamic response capability of the PEMFC technology.

The reference power signal for the PEMFC is given by the addition of the power set-point $p^{\mathrm{FC}}_{\mathrm{set}}$ and the signal provided by the secondary voltage controller $p^{\mathrm{FC}}_{\mathrm{sec}}$,

$$p^{\mathrm{FC}}_{\mathrm{ref}} = p^{\mathrm{FC}}_{\mathrm{set}} + p^{\mathrm{FC}}_{\mathrm{sec}} \tag{8}$$

C. Secondary Voltage Controller

The secondary control loop restores the primary power reserve provided by the BESSs. The measured voltage deviation at the main dc bus is integrated and the control signal is dispatched through the PEMFCs with a participation factor $\lambda^{\mathrm{FC}}_{k}$

$$p^{\mathrm{FC}}_{\mathrm{sec}} = \frac{K_{\mathrm{i}}}{s} \lambda^{\mathrm{FC}}_{\mathrm{k}} \left(v_{\mathrm{nom}} - v \right) \tag{9}$$

$$\lambda^{\mathrm{FC}}_{k} = \frac{P^{\mathrm{FC}}_{k}}{\sum_{j=1}^{N} P^{\mathrm{FC}}_{j}} \tag{10}$$

where, K_{i} is the integral controller gain and N is the number of PEMFCs participating to the secondary control. All the study cases in this paper consider all the PEMFCs participating (i.e., $N = 3$).

Table III
CONTROLLERS PARAMETERS.

Parameter	Value
$K^{\mathrm{B}}_{\mathrm{p}}$	2.0
$K^{\mathrm{B}}_{\mathrm{i}}$	1.0
$K^{\mathrm{FC}}_{\mathrm{p}}$	1.2
$K^{\mathrm{FC}}_{\mathrm{i}}$	10
K_{i}	7
D_{v}	0.01

IV. STUDY CASE

The control strategy is validated by different simulations in different mission conditions in DIgSILENT PowerFactory simulation environment. For sake of clarity the two most significant ones are here reported. The first one is used to show the control strategy approach and to validate it, while the second one is used to show and verify its performance in a real operating condition.

A. Control Strategy Validation

Figure 4 shows the results of the "synthetic" study case used for validation (from top to bottom: dc-bus voltage, powers of BESSs and PEMFCs, SOC, and load request). The system is

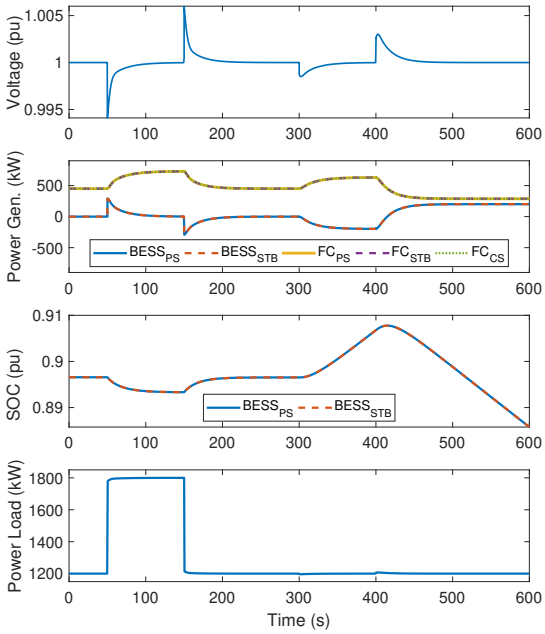

Figure 4. Results of the setup simulation.

supposed to be initially operating with a load of 1200 kW and with BESSs power set to 0 kW. At 50 s and 150 s load changes to 1800 kW and back to 1200 kW (to mimic propulsion power request). At 300 s and 400 s BESSs power set-point is changed from 0 kW to −200 kW and then to 200 kW in order to show the capability to manage SOC according to a predefined

strategy. SOC management is out of scope of this work but it is clear that it should be properly controlled. It can be noticed that the dc-bus voltage is controlled in primary regulation by the two BESSs and in secondary by the PEMFCs. By analyzing the powers is clear that the primary voltage control acts on the BESSs dc-dc converter in order to suddenly increase or decrease the power as soon as the load event happens. Thus, the secondary control modifies the PEMFCs power set-points to slowly increase their power outputs and return the BESSs back to the initial powers. The control strategy behaves as expected, with a transient support of the BESSs and a long-term regulation of the PEMFCs.

B. Real Load Simulation

For this simulation a real load profile of a ferry vessel has been considered [12] and, in particular, a specific transition among different operating scenarios for more than $30\,\mathrm{min}$. The selected load profile is a typical ferry condition in navigation ($0\,\mathrm{s}$–$400\,\mathrm{s}$), maneuvering ($500\,\mathrm{s}$–$600\,\mathrm{s}$), docking ($600\,\mathrm{s}$–$1000\,\mathrm{s}$) and, again, navigation ($1000\,\mathrm{s}$–$2000\,\mathrm{s}$) with a different speeds. The two BESSs deliver $100\,\mathrm{kW}$ each, due to the high load conditions, while the PEMFCs are controlled to cover the rest of the load power. Figure 5 shows the results of this simulation (from top to bottom: dc-bus voltage, powers of BESSs and PEMFCs, and load request including both propulsion and hotel loads). It is clear that the results of the combination of PEMFCs and BESSs show the ability to support the load variations with very good dynamic performances. All the fast variations are taken in charge by BESSs while PEMFCs follow the slow variations of the load according to the participation factors and the controller gains.

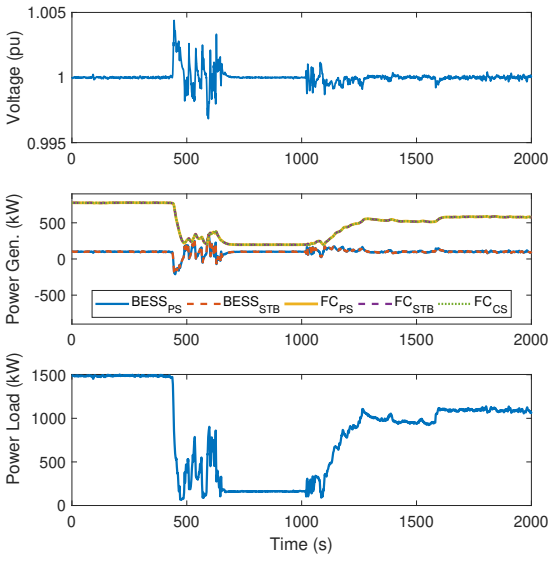

Figure 5. Results of the real load simulation.

V. Conclusion

This work presented a control strategy for the integration of fuel cells and battery energy storage systems into a dc shipboard power system. This methodology has been developed in a flexible and general way based on the primary and secondary frequency regulation of ac systems. The validation carried out on a real case study highlighted the possibility to manage significant load variations and to allow an environmentally friendly approach to marine sector with respect to the actual traditional power generation systems based on diesel engines.

Future studies will consider the implementation of an energy management algorithm to properly manage the energy storage devices and evaluate the savings with respect to a traditional solution in terms of CO_2 emissions.

References

[1] J. S. Thongam, M. Tarbouchi, A. F. Okou, D. Bouchard, and R. Beguenane, "All-Electric Ships-A Review of the Present State of the Art," in *Eighth International Conference and Exhibition on Ecological Vehicles and Renewable Energies (EVER)*, 2013.

[2] S. G. Jayasinghe, L. Meegahapola, N. Fernando, Z. Jin, and J. M. Guerrero, "Review of Ship Microgrids: System Architectures, Storage Technologies and Power Quality Aspects," *Inventions*, vol. 2, no. 1, pp. 1–19, Jun. 2017.

[3] J. J. Justo, F. Mwasilu, J. Lee, and J.-W. Jung, "AC-microgrids versus DC-microgrids with distributed energy resources: A review," *Renewable and Sustainable Energy Reviews*, vol. 24, pp. 387–405, Aug. 2013.

[4] K. Satpathi, V. M. Balijepalli, and A. Ukil, "Modeling and Real-Time Scheduling of DC Platform Supply Vessel for Fuel Efficient Operation," *IEEE Trans. Transport. Electrific.*, vol. 3, no. 3, pp. 762–778, Sep. 2017.

[5] K. Satpathi, A. Ukil, N. Thukral, and M. A. Zagrodnik, "Modelling of DC shipboard power system," in *IEEE International Conference on Power Electronics, Drives and Energy Systems (PEDES)*, 2016, pp. 1–6.

[6] K. Satpathi, A. Ukil, and J. Pou, "Short-Circuit Fault Management in DC Electric Ship Propulsion System: Protection Requirements, Review of Existing Technologies and Future Research Trends," *IEEE Trans. Transport. Electrific.*, vol. 4, no. 1, pp. 272–291, Mar. 2018.

[7] R. Lazzari, L. Piegari, S. Grillo, M. Carminati, E. Ragaini, C. Bossi, and E. Tironi, "Selectivity and security of DC microgrid under line-to-ground fault," *Electr. Pow. Syst. Res.*, vol. 165, pp. 238–249, Dec. 2018.

[8] S. Grillo, V. Musolino, L. Piegari, E. Tironi, and C. Tornelli, "DC Islands in AC Smart Grids," *IEEE Trans. Power Electron.*, vol. 29, no. 1, pp. 89–98, Jan. 2014.

[9] V. Nasirian, A. Davoudi, F. Lewis, and J. Guerrero, "Distributed adaptive droop control for DC distribution systems," *IEEE Trans. Energy Convers.*, vol. 29, no. 4, pp. 944–956, Dec. 2014.

[10] C. Li, J. Vasquez, and J. Guerrero, "Convergence analysis of distributed control for operation cost minimization of droop controlled DC microgrid based on multiagent," in *IEEE Applied Power Electronics Conference and Exposition, APEC*, 2016, pp. 3459–3464.

[11] J. P. Fernández-Porras, S. Grillo, F. D'Agostino, and F. Silvestro, "Mitigation of Voltage Deviations in DC Shipboard Microgrids Through the Active Utilization of Battery Energy Storage Systems," in *Power and Energy Society General Meeting (PESGM)*, Aug. 2018, pp. 1–5.

[12] E. Skjong, T. A. Johansen, M. Molinas, and A. J. Sørensen, "Approaches to Economic Energy Management in Diesel-Electric Marine Vessels," *IEEE Trans. Transport. Electrific.*, vol. 3, no. 1, pp. 22–35, Jan. 2017.

[13] S. Chowdhury and P. Crossley, *Microgrids and active distribution networks*. The Institution of Engineering and Technology, 2009.

[14] EG&G Technical Services, Inc., "Fuel Cell Handbook," U.S. Department of Energy, Tech. Rep., Nov. 2004.

[15] S. Grillo, M. Marinelli, S. Massucco, and F. Silvestro, "Optimal management strategy of a battery-based storage system to improve renewable energy integration in distribution networks," *IEEE Trans. Smart Grid*, vol. 3, no. 2, pp. 950–958, Jun. 2012.

[16] O. Tremblay, L.-A. Dessaint, and A.-I. Dekkiche, "A Generic Battery Model for the Dynamic Simulation of Hybrid Electric Vehicles," in *IEEE Vehicle Power and Propulsion Conference*, 2007, pp. 284–289.